Cement and Concrete Research 40 (2010) 146–156

Contents lists available at ScienceDirect

Cement and Concrete Research

journal homepage: http://ees.elsevier.com/CEMCON/default.asp

Comprehensive phase characterization of crystalline and amorphous phases of a Class F fly ash

Ryan T. Chancey [a,*], Paul Stutzman [b], Maria C.G. Juenger [c], David W. Fowler [c]

[a] Nelson Architectural Engineers, Plano, TX 75093, USA
[b] National Institute for Standards and Technology, Gaithersburg, MD 20899, USA
[c] The University of Texas at Austin, Austin, TX 78712, USA

ARTICLE INFO

Article history:
Received 2 November 2008
Accepted 31 August 2009

Keywords:
Amorphous material (b)
Characterization (b)
Image analysis (b)
Fly ash (b)
SEM (b)
X-ray powder diffraction

ABSTRACT

A comprehensive approach to qualitative and quantitative characterization of crystalline and amorphous constituent phases of a largely heterogeneous Class F fly ash is presented. Traditionally, fly ash composition is expressed as bulk elemental oxide content, generally determined by X-ray fluorescence spectroscopy. However, such analysis does not discern between relatively inert crystalline phases and highly reactive amorphous phases of similar elemental composition. X-ray diffraction was used to identify the crystalline phases present in the fly ash, and the Rietveld quantitative phase analysis method was applied to determine the relative proportion of each of these phases. A synergistic method of X-ray powder diffraction, scanning electron microscopy, energy dispersive spectroscopy, and multispectral image analysis was developed to identify and quantify the amorphous phases present in the fly ash.

1. Introduction

Fly ash, a by-product of the coal-combustion process, is used in a wide variety of engineering applications but is most commonly used as an addition to, or in replacement of, portland cement in concrete [1]. To ensure production of quality concrete, its constituent materials must be properly characterized with respect to physical and chemical properties. Currently, fly ash is characterized based upon its bulk elemental composition, with little regard for the phases resulting from the combination of such elements. The objective of the research presented here is to refine microanalysis techniques, including Rietveld quantitative X-ray diffraction (RQXRD), scanning electron microscopy (SEM), energy dispersive spectroscopy (EDS), and multispectral image analysis (MSIA), to accurately characterize the crystalline and amorphous phases present in fly ash.

American Society for Testing and Materials (ASTM) C 618 defines two classes of fly ash based upon chemical and physical characteristics [2]. The chemical characterization is based upon bulk oxide content commonly obtained through X-ray fluorescence (XRF) analysis. ASTM C 618 Class F fly ash must contain a sum of SiO_2, Al_2O_3, and Fe_2O_3 contents equal to or greater than 70% by mass, while Class C fly ash must contain a sum of the same constituents equal to or greater than 50% by mass. However, the classes are commonly distinguished based solely upon CaO content, which may approach 20% for Class F ashes and 30 to 40% for Class C [3]. The increased CaO content in Class C fly ashes may be attributed to the presence of lime, crystalline tricalcium aluminate, belite, and/or alite.

Many variables affect the chemical composition, morphology, and relative phase proportions in fly ash. These variables include raw coal source and mineralogy, coal burning conditions, by-product collection method, and implementation of environmental hazard mitigation techniques. As coal is an inherently heterogeneous raw material, so is its combustion by-product, fly ash. As solid coal is heated in a furnace at operating temperatures of 1400 °C to 1600 °C, the clay minerals lose water and melt; the carbonates decompose to release CO_2 and form CaO and MgO; the sulfides are oxidized to form metallic oxides and sulfite; chlorides volatize to form HCl and sulfates; and silica remains chemically unaltered by the high temperatures [4]. The melting points of the clay minerals in coal are determined largely by their chemical composition, especially by the amount of glass modifying elements, or fluxing agents, present [5]. Coal minerals with larger concentrations of these fluxing agents will form a relatively larger amount of glass upon cooling than coal minerals with lower concentrations of the fluxing elements. Generally, amorphous material accounts for 60% to 90% of bulk fly ash composition, while crystalline material accounts for the difference [6].

Not only do the properties of fly ash vary between coal-fired power plants burning different coals, they may also vary over time within a single plant burning different coals, or even within a single plant burning the same coal, but under different conditions. Schlorholtz et al. [7] monitored the physical and chemical properties of fly ash produced at one electric generating station over a period of 2 years. The bulk chemical compositions of the ash samples did not differ greatly over the

* Corresponding author.
E-mail address: rchancey@architecturalengineers.com (R.T. Chancey).

0008-8846/$ – see front matter © 2009 Elsevier Ltd. All rights reserved.
doi:10.1016/j.cemconres.2009.08.029

sampling period; however drastic differences in physical performance were observed. Hydrated specimens of fly ashes sampled at different dates yielded vastly different compressive strengths. These differences were assumed to be a function of phase mineralogy.

1.1. Characterization of crystalline phases in fly ash

Fly ash typically contains a number of distinct crystalline phases, which comprise the bulk crystalline fraction. A few of these phases occur almost ubiquitously in fly ash. The more commonly occurring crystalline phases are quartz, mullite, hematite, ferrite spinels, anhydrite, melilite, merwinite, periclase, tricalcium aluminate, and lime. For a more detailed discussion of these phases, see [8] and [9].

The qualitative mineralogy of crystalline material in fly ash is well-documented [10,11] due to the relative simplicity of investigating materials with long-range molecular order. The vast majority of crystalline phase characterization has been carried out by X-ray diffraction; however, a few studies have used vibrational spectroscopy and selective dissolution techniques [4,12].

Efforts to quantify both the proportion of total crystalline phases to total amorphous phases and the relative proportions of the individual crystalline phases have proven a non-trivial task; however some reasonable results have been produced using semi-quantitative methods, such as the reference-intensity-ratio method [10,13,14]. These methods are not ideal for analysis of largely amorphous materials such as fly ash due to the difficulties in matching reference standards and peak intensity measurement.

Recently, a rigorous quantitative approach to crystalline phase analysis has been applied through the Rietveld quantitative X-ray diffraction (RQXRD) method [15]. Although originally developed for quantitative analysis of systems with few phases, the Rietveld method has been optimized for quantification of the multiple crystalline phases in fly ash. This has been made possible due to thorough qualitative characterization of the types of minerals typically present in fly ash and advanced computational capabilities. The Rietveld approach and analysis protocols were demonstrated through analysis of National Institute of Standards and Technology (NIST) standard reference materials [16]. Using the publicly available GSAS[1,2] code and a detailed analysis protocol, estimations of crystalline phase proportions were made for a variety of fly ashes and a database was compiled [17]. Furthermore, rigorous quantitative XRD studies have been conducted to investigate the relative proportion of pure iron oxide to the ferrite spinel phases present in fly ash [18]. These experiments have shown that the ferrite spinel phase fractions determined by RQXRD were within 10% of the same fractions as determined by magnetic measurements. Since the ferrite spinel phase rarely exceeds 5% of the total fly ash mass, these results demonstrate that relatively accurate estimations of minor constituent phase fractions may be carried out through RQXRD.

1.2. Characterization of amorphous phases in fly ash

The presence of amorphous material in fly ash was recognized in the 1950s and 1960s; however, chemical characterization of these phases was not attempted until the late 1980s [19]. Due to their structurally disordered nature, proper characterization of amorphous solids often proves more tedious than characterization of their crystalline counterparts. Most often, characterization of the amorphous fraction of fly ash is carried out on the bulk scale, yielding valuable information regarding the chemistry of the amorphous fraction as a whole, but offering little information regarding the heterogeneity of the amorphous fraction and characteristics of the discrete amorphous phases that exist.

Characterization of the amorphous phases of fly ash has been approached with limited success using a number of analytical techniques, each with inherent strengths and limitations. Many of these techniques have been discussed at length and numerous references are provided in [4], including polarized light microscopy, electron microscopy, X-ray diffraction, vibrational spectroscopy, gamma-ray spectroscopy, nuclear magnetic resonance spectroscopy, thermal analysis, and selective dissolution. An innovative computation technique is presented in [20].

2. Experimental methods

Each of the experimental methods described herein was employed to yield direct information regarding the chemical composition of discrete microphases in fly ash. Few standardized procedures exist for characterization of this heterogeneous material, thus existing procedures used for analysis of less complex systems were modified and new procedures were developed to facilitate proper characterization of both crystalline and amorphous microphases of fly ash. The experimental methods are described in great detail as they may serve as a platform against which new standard procedures can be developed.

2.1. Fly ash source

Due to the complexity of the experimental matrix, lack of standardized procedures, propensity for error propagation, and inherent variability of fly ash composition between sources, a single fly ash was used to develop procedures for microphase characterization and reactivity investigation. Although no single fly ash may be considered “typical”, one was carefully selected which exhibits a “middle of the line” bulk chemical composition, favorable physical properties, and benefits to both plastic and hardened concrete. The experimental procedures for microphase characterization and reactivity investigation were developed and refined using this “model” system, and later applied to other fly ashes. All samples used in these experiments were obtained from a single barrel of ash processed on July 7, 2005. The fly ash was tested for oxide composition using XRF, general morphology using scanning electron microscopy of polished cross sections and raw ash dusted on carbon tape, and particle size distribution using laser diffraction.

2.2. Identification and quantification of crystalline phases

The crystalline components of the fly ash were characterized using X-ray powder diffraction. Raw fly ash samples were prepared, scanned, and analyzed to identify the crystalline phases present. Subsequently, a suitable internal standard was intermixed with each sample and analyzed using a rigorous quantitative method to determine the relative proportions of each phase previously identified.

2.2.1. Data acquisition

The X-ray powder diffraction data were collected using a Siemens[3] D500 diffractometer with a 2200 W copper-target X-ray tube, operating at 40 mA and 30 kV. The diffractometer was configured with a 1° divergent slit, 4° soller slit, and 1° anti-scatter slit on the incident-beam side and a 1° anti-scatter slit, 4° soller slit, 0.15 mm receiving slit, and a 0.6 mm detector slit on the divergent-beam side. A graphite monochromator was used to prevent Cu K-β radiation from reaching the X-ray detector.

[1] Certain commercial equipment, instruments, or materials are identified in this report in order to specify the experimental procedure adequately. Such identification is not intended to imply recommendation or endorsement by the National Institute of Standards and Technology, nor is it intended to imply that the materials or equipment identified are necessarily the best available for the purpose.

[2] A.C. Larson and R.B. Von Dreele, General Structure Analysis System (GSAS), Los Alamos National Laboratory Report LAUR 86-748 (1994), http://www.ccp14.ac.uk/solution/gsas/.

[3] http://www.bruker-axs.de.

2.2.2. Sample preparation

1.35 g of fly ash was placed into a ceramic mortar along with 0.15 g of 99.9% pure rutile (TiO_2) as an internal standard. Ethanol was added to the powder while blending the mixture using a pestle, forming a homogeneous slurry. The powder was then rigorously ground by hand for approximately 3 min, allowed to dry at 40 °C for 1 h, and brushed from the mortar onto weighing paper. The grinding served not only to thoroughly mix the rutile and fly ash, but also to optimize the particle size of the mixture for X-ray diffraction analysis.

The powder sample was transferred into a standard top-load style, plastic sample holder and evenly distributed. This holder type was chosen due to the absence of low-angle X-ray scatter experienced when using metal back-load holders. The sides of the powder were struck flush with the holder, leaving an approximately 1 cm^2 mound in the center. A glass platen was then placed onto the sample, compressing the powder into the holder. Enough pressure was applied such that the powder sample remained cohesive when the sample holder was tilted approximately 75° about both in-plane axes. Care was taken to use only vertical pressure on the platen, preventing rotation and translation of the platen and holder, to minimize preferential orientation of crystalline material in the sample.

2.2.3. Experimental conditions

Samples were scanned from 10° to 70° 2θ in increments of 0.02° with a step-time of 8 s/step. Each scan lasted approximately 7 h. Such lengthy scans were necessary in this case due to the relatively small bulk proportion of crystalline material and the desire to resolve both major and minor crystalline phases in a manner favorable for rigorous quantitative analysis.

2.2.4. Qualitative data analysis

Qualitative analysis was performed using two commercially available software packages. The general shape of the base of the diffraction curve, or pattern "background," was identified and fit analytically through the software's implementation of either cubic spline or shifted Chebyschev polynomial functions, depending on the shape of the background curve. This background, including the broad "hump" caused by the amorphous ash fraction, was numerically subtracted from the base pattern, resulting in well-defined diffraction peaks representative of the crystalline phases present.

The 1996 version of the International Center for Diffraction Data (ICDD) Powder Diffraction File PDF 2[4] was employed by each software suite for comparison of reference diffraction patterns of known inorganic crystalline phases to those obtained experimentally. Prior to phase identification, the pattern was corrected for x-axis (2θ) shift caused by sample height displacement error. The diffraction peak locations were then compared to those of the reference patterns of minerals commonly found in fly ashes. Following a potential peak-location match of the primary peak for a phase, the secondary and tertiary peaks were identified. A phase was considered present if the three experimentally determined peaks of highest intensity matched the respective reference peak locations, though occasionally for some low-concentration constituents fewer peaks were available for identifications. Given the high intensity of the X-ray scans, peaks were resolved which represent only minor contributions to the bulk, but were included in the detailed analysis.

2.2.5. Quantitative data analysis

Following comprehensive qualitative identification of the crystalline phases present in the fly ash, their relative proportions were determined through Rietveld QXRD. Additionally, the bulk amorphous fraction was determined by difference through the use of the internal standard. An academic version of TOPAS,[5] a commercially available software package, was used to perform the Rietveld quantitative analysis.

[4] International Center for Diffraction Data Powder Diffraction File, http://www.icdd.com.

[5] TOPAS-Academic, Coelho Software, Brisbane, Australia, http://members.optusnet.com.au/~alancoelho/.

Quantitative analysis was performed on the raw, unprocessed diffraction data. The Rietveld whole-pattern, least-squares fitting routine was applied to the data from 15° to 65° 2θ. Inclusion of data less than 15° 2θ did not improve the background fit nor include peaks of any phases present. Inclusion of data greater than 65° 2θ included only peaks for the internal standard, already accounted for by lower-angle peaks of suitable resolution.

The Rietveld method employs an algorithm based upon parameters derived from theoretical crystal structures [21–23]. Actual crystal structure parameters may differ from the theoretical parameters, especially in materials subjected to high temperature, as in the case of fly ash. Thus, a parametric "refinement" was necessary to accurately fit a calculated pattern to the experimental data. The refinement procedure entailed performing an initial fit, holding all parameters fixed. Then, beginning with the predominant phase, each relevant parameter was varied within an acceptable range, while holding all other parameters fixed, to determine which favorably affected the fit for that phase. The parameters varied for each phase were largely dependent on a visual assessment of diffraction peak shape and magnitude. Once an acceptable fit was achieved for a phase, all parameters of that phase were again fixed, and the next predominantly-occurring phase was refined. This process was repeated until statistical improvements in curve fit were negligible.

Rietveld analysis of the diffraction data yielded approximations of relative proportions of the discrete crystalline phases in the fly ash. However, such analysis is based upon the pretense that the bulk material is largely crystalline, and thus results are based upon 100% crystalline sample composition. The crystalline phase fractions were easily normalized to the bulk crystalline fraction through the use of a carefully-measured addition, or "spike", of internal standard. Each phase fraction was normalized to the known mass spike of internal standard according to Eq. (1):

$$P_i' = P_i\left(\frac{I'}{I}\right) \tag{1}$$

where P_i' is the mass percentage of phase i present in the spiked sample, P_i is the mass percentage of phase i as determined directly by Rietveld analysis, I' is the known mass percentage of internal standard, and I is the mass percentage of internal standard as determined directly by Rietveld analysis.

Following normalization to the known mass of internal standard, the sum of the spiked phase fractions still included the original mass of internal standard. To obtain the phase fractions of the original material constituents, without the inclusion of the internal standard, the spiked phase fractions were again normalized according to Eq. (2):

$$P_i'' = P_i'\left(\frac{100}{100-I'}\right) \tag{2}$$

where P_i'' is the mass percentage of phase i present in the original sample. Subsequently, the total amorphous fraction can be calculated by difference, as shown in Eq. (3):

$$P_{am} = 100-\sum P_i'' \tag{3}$$

where P_{am} is the mass percentage of amorphous material present in the original sample.

2.3. Identification and quantification of amorphous phases

The amorphous fraction of the fly ash was characterized using scanning electron microscopy (SEM), energy dispersive spectroscopy (EDS), and multispectral image analysis (MSIA). Fly ash samples were carefully prepared before undergoing X-ray microanalysis via SEM/EDS, resulting in high-resolution images of the spatial distribution of elements in each sample. Digital image overlays were created to

facilitate qualitative determination of element combinations, or compounds. The individual images were mathematically linked to form a multispectral image suitable for segmentation into individual phases, and the relative abundance of each phase was subsequently quantified.

2.3.1. Sample preparation

For proper scanning electron and X-ray microanalysis, a polished cross section of the sample must be prepared, such that electron beam-sample interaction height is uniform across the sample area. A typical polished SEM sample consists of a subject material mixed with or embedded in a molded epoxy disk measuring 31.75 mm in diameter and approximately 12 mm in height. To allow for analysis of less than 0.5 g of sample, a modified disk mount was fabricated from a blank, standard size epoxy disk. Epotek 353ND[6] epoxy was chosen due to its favorable thermal properties for high-intensity SEM analysis. Furthermore, it exhibited a better particle–epoxy bond than other common epoxies. After thorough mixing of the two-part epoxy, 11 g of the epoxy was dispensed into a standard plastic sample mold coated with a bond-breaking agent, taking care to avoid entrapped air bubbles. The epoxy was not vacuum-cured due to its low boiling point. Instead, the epoxy disks were heat-cured for 24 h at 40 °C and standard pressure before curing at 23 °C and standard pressure for an additional 24 h. The hardened epoxy disks were then carefully removed from the plastic mold.

The blank epoxy disks were then machined using a computer numerically controlled (CNC) mill to the dimensions in Fig. 1. The height of each disk varied slightly with respect to the others due to differences in preparation and curing, however this did not affect the analysis as long as the height of each disk was constant throughout its own area. Following fabrication, the disks were cleaned in an ultrasonic bath of ethanol to eliminate loose particles.

For each fly ash sample, a fly ash/epoxy mixture was made at a ratio of 2:1 by mass. A particle-rich mixture without particle agglomerations was desired. Therefore, the mixture had to be sufficiently dilute to properly disperse the powder and provide inter-particle separation. The fly ash to epoxy ratio is a function of the properties of material to be suspended, thus experimentation may be necessary to determine the optimal mixture proportions for other fly ashes.

The fly ash and epoxy were thoroughly but gently mixed with a glass stirring rod to provide adequate particle dispersion without air entrapment. Approximately 0.5 ml of the mixture was placed into each of the wells on the epoxy disk, allowing some material to protrude above the hardened epoxy surface, but preventing the samples from contacting one another. Any well not filled with the fly ash/epoxy mixture was filled with pure liquid epoxy. The completed epoxy disk was again cured for 24 h at 40 °C and standard pressure before curing at 23 °C for an additional 24 h.

Once hardened, the sample surface was ground flush using #60 grit silicon carbide grinding paper. All grinding was performed by hand, without aid of an automatic grinder. Great care was taken to prevent particle "plucking" from the sample surface. During grinding, slight downward pressure was exerted on each disk. The sample was rotated approximately 45° in plane every 30 s during grinding. After achieving a flush surface using #60 grit paper, grinding was continued using progressively finer grit paper in the following succession: #180, #400, #600, #800, and #1200. Each successively finer paper was used until the scratches on the surface of the sample were of uniform width. This could be approximated with the naked eye; however an optical stereomicroscope was used in many cases. Grinding at each fineness lasted approximately 5 min. The sample was lightly washed with ethanol and dried with compressed air after each grinding.

After grinding, each sample was polished using successively finer diamond paste in the following succession: 6 μm, 3 μm, 1 μm, 0.5 μm, and 0.25 μm. The polishing was performed using a small amount of diamond paste applied to optical-grade cloth mounted upon a motorized polishing platen rotating at 90 rpm. Pressure was applied in a manner similar to that of grinding; however the sample was continuously rotated in an orbital motion. That is, the polisher rotated the sample about the axis of the platen, contrary to the direction of rotation of the platen, while also rotating the sample about its in-plane axis. Again, polishing at each fineness lasted approximately 5 min, and the optical cloth was replaced after each polishing step. Following the final polishing, the sample was cleaned with ethanol and a clean optical cloth. The samples were stored in a vacuum desiccator until needed.

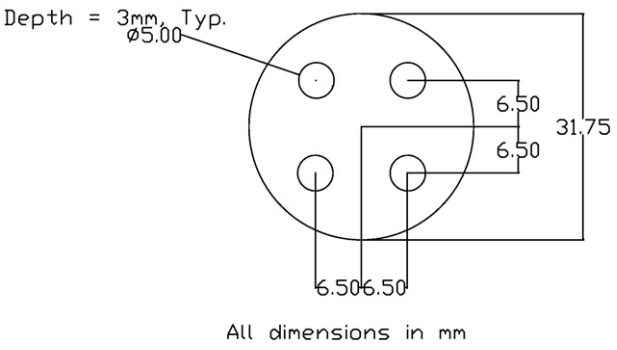

Fig. 1. Schematic of SEM sample disk.

Finally, the samples were coated with a conductive medium to provide electronic continuity from the electron beam to a ground source. Carbon was chosen as the coating material, since it does not interfere with X-ray microanalysis. Heavier elements such as gold, palladium, and silver are also commonly used as conductive coatings and were investigated. Of those, only silver yielded acceptable results, though the backscatter flux is reduced and other metals interfere with EDS analysis through peak interference and reduced X-ray flux due to absorption. 25 nm of carbon was deposited on the sample surface using a vacuum carbon evaporator. The coating thickness was measured using the brass substrate method [24].

2.3.2. Experimental conditions

Optimum conditions for data acquisition were determined through trial analyses, such that X-ray intensity was maximized. The SEM was operated at an accelerating voltage of 15 kV, nearly twice the X-ray excitation energy of iron, the heaviest element to be investigated. The 2× minimum over-voltage was suggested by Goldstein [25]. The lowest feasible voltage was used to prevent localized heating and subsequent destruction of the epoxy-bound sample. The largest available aperture, 120 μm, was used, and working distance which maximized X-ray intensity was found to be 11 mm.

The EDS was configured for collection of high-resolution element maps of 1024 pixels^2 with pixel dwell time of 400 μs/pixel. The atypically short dwell time was utilized to minimize local charging effects, subsequent beam drift, and image deformation. Under this configuration, the X-ray count rate was approximately 10,000 counts/s and the processor time constant was set at 4.0 to limit X-ray detector dead time to 15%. Element maps for silicon, calcium, aluminum, iron, potassium, magnesium, and sodium were simultaneously collected. One frame of an image set was collected in approximately 8 min. The intensity of the X-ray signals, and thus image maps, were insufficient for analysis after a single frame; therefore the multi-scan EDS function was utilized to collect a series of frames of the same sample area over a period of time. Tests were conducted and the minimum number of frames needed for proper analysis was found to approach 30. Conservatively, 50 frames were collected for each sample, resulting in scans of approximately 7 h each. For uniformity, the system was configured identically for image collection of each sample.

[6] Epoxy Technology Inc., Billerica, MA, http://www.epotek.com.

2.3.3. Data analysis

Following collection of the high-resolution element maps, careful qualitative analysis was performed to identify amorphous phases present in the fly ash. Subsequently, rigorous quantitative analysis was performed to determine the respective area fractions of each phase, which was correlated to a volume fraction, and a mass fraction was approximated. Both qualitative and quantitative image analyses were performed using MultiSpec,[7] using procedures modified from those of Lydon [26].

2.3.3.1. Qualitative analysis. The individual element maps for each image field were processed, then mathematically linked to form a single multispectral image suitable for analysis. Each image was preprocessed to maximize the signal/noise ratio before higher-level processing was attempted. Using ImageJ,[8] a median filter was applied to every image in each set to reduce speckling, or the "salt-and-pepper" effect by replacing each pixel with the median of the neighboring pixel values [27]. A median filter of radius 1 was chosen due to its ability to reduce image noise without blurring edges or boundaries.

Following application of the median filter, further background noise was eliminated from the image by removing the faint signals, which were not attributable to any particular larger particle in the image. Since all images were collected under similar conditions, this preprocessing method was standardized and identical procedures applied for each image set. Inspection revealed that images of minor constituent elements contained more noise than those of the major constituent elements, and further experimentation confirmed the necessity to clip greater amounts of background from the images of minor elements. Based on the standard pixel-brightness scale of 0–255, with 0 representing a completely black pixel and 255 representing a completely white pixel, those pixels with values less than threshold values were removed from the respective images. Details regarding threshold values for each element map may be found in [8]. This minimum threshold value manipulation was accomplished using the Image Adjustment–Brightness/Contrast feature of ImageJ. The actual values may vary with the image collection scheme and equipment used. Following the image preprocessing, the individual element images were linked to form a multispectral image in accordance with procedures of Lydon [26].

2.3.3.2. Quantitative analysis. The determination of the mass fractions of the amorphous phases required some data manipulation, as the multispectral image analysis yields phase fractions in terms of area, not volume or mass. The area fraction of each phase was first directly correlated to a volume fraction due to the predominantly spherical and symmetrical shape of the amorphous particles [28], such that Eq. (4) applies:

$$a_i = v_i \tag{4}$$

where a_i is the area fraction of phase i and v_i is the volume fraction of phase i. As mentioned, some crystalline phases were observed to assume an angular, dendritic, or needle-like form, and are thus non-symmetrical. The effect of the shape of these minor constituents on the overall analysis was considered and determined insignificant since the non-spherical shapes were assumed to be randomly oriented in the sample.

The volume fraction of each phase was then correlated to a mass fraction following Eq. (5):

$$m_i = v_i \delta_i \tag{5}$$

[7] Multispec image data analysis system. http://cobweb.ecn.purdue.edu/~biehl/MultiSpec/.

[8] ImageJ image processing and analysis, http://rsbweb.nih.gov/ij/.

Table 1
Crystalline phase densities (g/cm^3).

Crystalline phase	Density
Quartz	2.64
Ferrite spinel/maghemite	5.18
Periclase	3.58

where δ_i is the density of phase i. Recognizing the differences in density due to particle morphology and chemistry [29], the inter-particle variation was considered sufficiently small to assume a bulk amorphous density of 2.5 for non-alkali-modified glasses and 2.4 for alkali-modified glasses, based on work by Hemmings and Berry [30] and Pietersen [5]. The crystalline phase densities were taken as listed in Table 1.

The mass fraction data were compiled, and the crystalline mass fractions obtained from the SEM/MSIA technique were compared to those obtained from the RQXRD technique. Following this comparison, the crystalline phases were excluded from the SEM/MSIA data for simplicity. The crystalline phases resolved through EDS mapping; maghemite–ferrite spinel, periclase, and quartz, were excluded from the data set, and the remaining phases were normalized to 100% according to Eq. (6):

$$n_{am,i} = \left(\frac{100}{100 - a_{cr}}\right) a_{am,i} \tag{6}$$

where $n_{am,i}$ is the normalized area fraction of amorphous phase i, a_{cr} is the total area fraction of the crystalline phases, and $a_{am,i}$ is the reported area fraction of amorphous phase i. The resulting data yielded a comprehensive characterization of the amorphous phases in the fly ash.

3. Results and discussion

3.1. Bulk chemical properties

The chemical analysis of the fly ash by X-ray fluorescence spectroscopy is presented in Table 2. The sum of the SiO_2, Al_2O_3, and Fe_2O_3 fractions was 83.71%, thus the fly ash is classified according to ASTM C 618 as "Class F". The fly ash contained 9.90% CaO, which is a mid-range proportion among Class F fly ashes. The loss on ignition (LOI), an indication of unburned carbon, was 0.11%, a relatively low value among all fly ashes. The reported moisture content was 0.07%. The bulk chemical analysis was performed by the manufacturer in accordance with ASTM C 618, and the sum of the elemental oxides does not equal 100% due to the presence of unreported trace elements [31,32].

3.2. Physical properties

The manufacturer reported the bulk density of the fly ash as 2.39 g/cm^3, and the majority of the fly ash particles were found to be spherical and unbroken when examined using both optical and scanning electron

Table 2
Bulk chemical analysis of a Class F fly ash.[a]

Oxide	Mass %
Silicon dioxide (SiO_2)	55.11%
Aluminum oxide (Al_2O_3)	20.42%
Iron oxide (Fe_2O_3)	8.18%
Magnesium oxide MgO	2.72%
Sulfur trioxide (SO_3)	0.54%
Calcium oxide (CaO)	9.90%
Available alkalis as Na_2O_e	0.46%
Loss on ignition (LOI)	0.11%

[a] Based upon a single analysis.

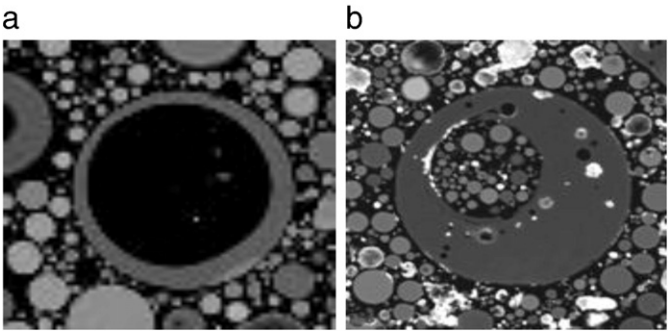

Fig. 2. SEM images of a cross section of a (a.) cenosphere and (b.) plerosphere.

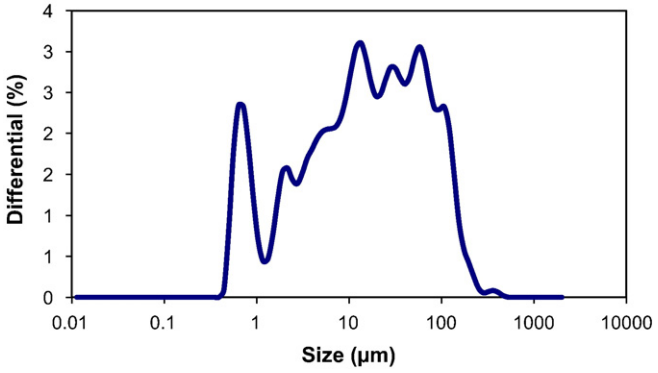

Fig. 3. Differential particle size distribution of the subject fly ash.

microscopes. Some angular particles were observed; with the longest dimension of most being between 25 μm and 35 μm. Microscopic analysis of polished cross sections revealed that most of the spherical particles were entirely solid; however some cenospheres and plerospheres were present in each sample. Cenospheres are particles with a largely empty hollow core, while plerospheres are particles with a hollow core that is noticeably filled with other fly ash particles. SEM images of a cross section of a cenosphere and a plerosphere are shown in Fig. 2a and b, respectively. All angular particles were entirely solid.

Particle size distribution was measured using laser diffraction. The mean particle size is approximately 14 μm, the smallest particles approximately 0.4 μm, and the largest particles approximately 520 μm. It should be noted that only 4% of the particles, by mass, were larger than 121 μm. The differential particle size distribution, as measured by laser diffraction, is presented in Fig. 3. The differential particle size distribution curve shows the fraction of material at a given particle size.

3.3. Identification and quantification of crystalline phases

Peaks representing quartz, mullite, maghemite, periclase and rutile (the added internal standard) were easily identified in the diffraction pattern. Some poorly-defined peaks corresponded to reported peak locations for ettringite. Given that calcium aluminates may hydrate in the presence of sulfates to form ettringite, its presence in the fly ash was considered. Storage conditions for fly ash may facilitate this hydration, as reactive calcium aluminates and calcium sulfates may react upon wetting to form secondary products.

The diffractogram for the fly ash + internal standard mixture is shown in Fig. 4. The representative diffraction peaks for each phase are labeled. The locations of the primary, secondary, and tertiary representative peaks, as reported in the ICDD Powder Diffraction Database, are listed in Table 3, although not all of these peaks were necessarily evident in the experimental pattern for low-concentration phases exhibiting very weak peaks. The broad hump, or "halo", centered at approximately 26.5° 2θ on the diffractogram suggests the presence of a large amount of amorphous material. In some preliminary samples, traces of anatase, a low-temperature polymorph of rutile, was found. Fortunately, this was discovered before most of the samples had been prepared with the internal standard. The laboratory supply of rutile was heat-treated in an oven at 900 °C for 2 h to convert the anatase back into the high-temperature rutile polymorph. Subsequent diffraction analysis confirmed the absence of anatase from the internal standard.

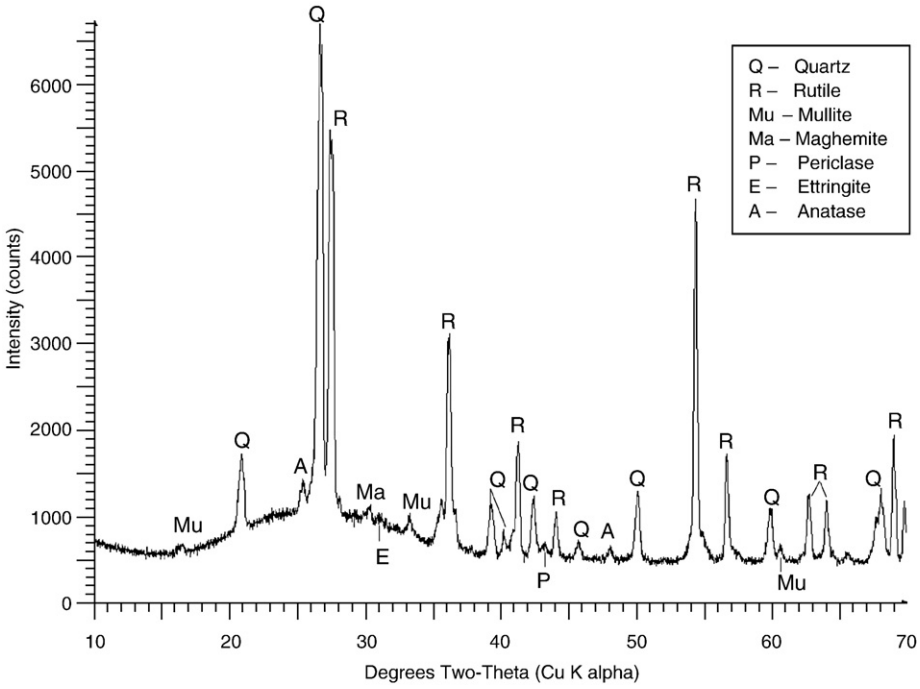

Fig. 4. Diffractogram of a Class F fly ash with representative peaks labeled.

Table 3
Reported peak locations for phases present in a Class F fly ash prepared with an internal standard (rutile) [33].

Phase	Peak location (°2θ, Cu Kα)		
	Primary	Secondary	Tertiary
Quartz	26.640	20.859	50.141
Rutile	27.447	54.323	36.086
Mullite	26.268	25.971	40.875
Maghemite	35.631	30.241	62.926
Periclase	42.917	62.303	109.764
Ettringite	9.091	15.784	22.944

Table 4
Relative proportions of crystalline phases and bulk amorphous material present in a Class F fly ash based upon Rietveld X-ray powder diffraction.

Phase	Relative amounts in samples (%)					Mean	Std. dev.
	1	2	3	4	5		
Quartz	16.8	16.9	16.0	16.2	15.9	16.4	0.4
Mullite	3.6	3.5	3.8	3.7	3.6	3.6	0.1
Maghemite	2.1	2.2	1.9	2.2	2.2	2.1	0.1
Periclase	0.34	0.38	0.35	0.38	0.36	0.36	0.02
Ettringite	0.22	0.19	0.16	0.21	0.22	0.20	0.03
Amorphous	77.0	76.8	77.8	77.3	77.8	77.3	0.5

Following qualitative determination of the phases present in the subject fly ash, five samples were prepared and analyzed and the relative proportions of the crystalline phases present were determined using Rietveld QXRD. Multiple samples were analyzed to assess the level of precision to which each of the phase fractions could be quantified. Each sample was taken from the same batch of fly ash, and was prepared independently of the others to account for error introduced through variability in sample preparation. The proportions of each of the crystalline phases and the bulk amorphous material determined for each of the five samples are reported in Table 4, along with the mean value and standard deviation for each phase.

3.4. Identification and quantification of amorphous phases

The presence and relative proportions of all amorphous and some crystalline phases present in the subject fly ash were determined through scanning electron microscopy (SEM), energy dispersive spectroscopy (EDS), and multispectral image analysis (MSIA) techniques. Considering the interdependence of these three methods, they will collectively be referred to as "MSIA".

3.4.1. Qualitative results

Fig. 5 shows the raw element maps, as collected by the SEM/EDS system. Each image was preprocessed as described earlier and the elemental images were linked to form a multispectral image stack, indicative of the phases present in the sample. One presentation of the stacked image is shown in Fig. 6. Overlays of only three elements may be displayed simultaneously, one each in red, green, and blue. Mutually exclusive combinations of these colors indicate individual material phases. Fig. 6 shows an overlay of silicon, calcium, and aluminum.

Following combination of the elemental images, the multispectral image was visually inspected to roughly assess which phases may be present. A silicon-rich phase containing almost no impurities was common (bright green in Fig. 6). This phase exclusively featured angular boundaries, and thus was identified as crystalline quartz. Iron and magnesium rich phases were identified as maghemite (a ferrite spinel) and periclase, respectively, due to their lower abundance and definitive morphology.

A number of additional color combinations, and thus material phases, were evident in the image. For example, in Fig. 6 a phase which appears orange is a combination of green and blue channels;

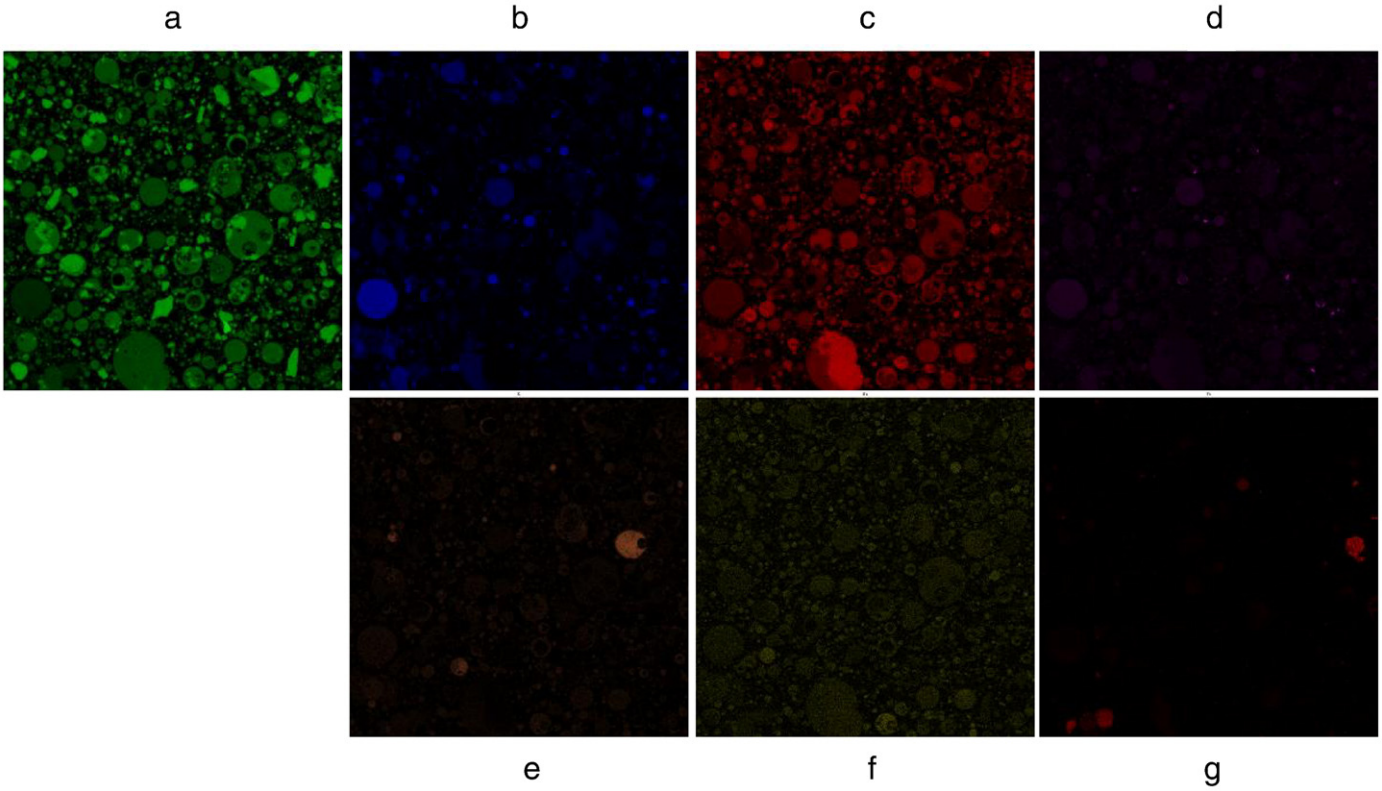

Fig. 5. Raw element maps of a Class F fly ash. (a.) Silicon, (b.) calcium, (c.) aluminum, (d.) magnesium, (e.) potassium, (f.) sodium, (g.) iron, field width = 2050 μm.

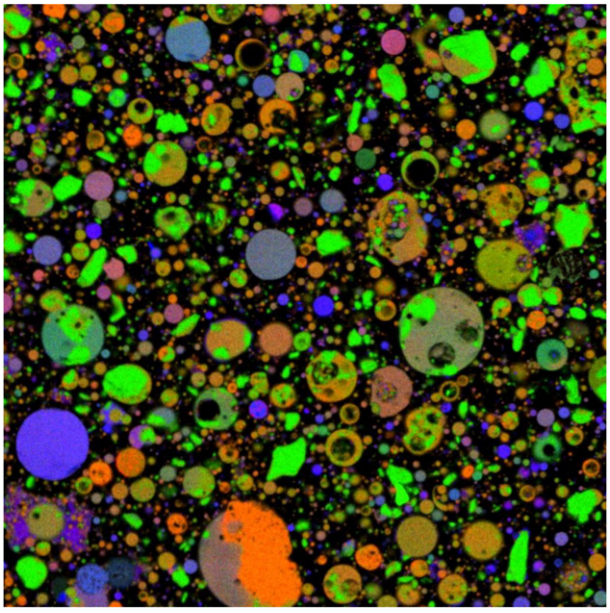

Fig. 6. Multispectral overlay of aluminum, silicon, and calcium (red, green, and blue, respectively) highlights compositionally distinct regions. Field width = 2050 μm. (For interpretation of the references to color in this figure legend, the reader is referred to the web version of this article.)

the silicon and calcium images. Furthermore, a phase which appears greenish-purple is a combination of red, blue, and green channels; the aluminum, calcium, and silicon images. Given the spherical morphology of the particles, it was assumed that these phases were calcium silicate glasses and calcium–aluminosilicate glasses, respectively.

To supplement the purely visual qualitative analysis, a semi-quantitative multispectral approach was applied using the MultiSpec program. Following procedures of Lydon [26], an unsupervised clustering analysis was performed to identify the number of statistically determinable mutually exclusive phases. This was an iterative approach, requiring the user to input the number of phases, or clusters, into which the image will be segmented. For the first iteration, 21 clusters were specified, as this is three times the number of channels used to form the multispectral image, as suggested by Lydon. The analysis resulted in 21 phases being defined, with most having area fractions less than 3%, and some having area fractions less than 1%. A "principal components analysis", performed within MultiSpec, revealed the relative contributions of each channel, or element, to each phase. Many of the defined phases appeared to be of very similar composition. The focus of this work is to define major phase delineations; thus, the number of clusters was iteratively decreased until substantial compositional differences were noted through the principal components analysis. A visual inspection was conducted to ensure that the clusters suggested by MultiSpec were similar to those visually discernable in the image stack.

Eight mutually exclusive phases were visually and statistically discernable through the analysis of the multispectral image. Quartz, periclase, and maghemite were identified as crystal phases due to their distinct composition and morphology and the lack of minor elements occurring in those phases. The remaining five phases were classified as amorphous phases due to their spherical morphology, indicating rapid cooling in the flue gas stream. The approximate composition of these phases was determined through visual image-stack analysis and computerized principal components analysis. Three phases contained primarily calcium, aluminum, and silicon, but each phase exhibited distinctly different proportions of those elements. One phase contained primarily potassium, aluminum, and silicon; another contained primarily sodium, aluminum, and silicon. Following the glass-polymerization principles detailed in [5,8], the amorphous phases were classified into the following five groups:

- Calcium-Modified Aluminosilicate #1 (C-A-S 1)
- Calcium-Modified Aluminosilicate #2 (C-A-S 2)
- Calcium-Modified Aluminosilicate #3 (C-A-S 3)
- Potassium-Modified Aluminosilicate (K-A-S)
- Sodium-Modified Aluminosilicate (N-A-S)

In all of these cases, aluminum has likely served as a polymeric network addition to pure silica glass, resulting in aluminosilicate glass. Subsequently, a modifier cation, either Ca^{2+}, K^{+}, or Na^{+}, balanced the non-bridging oxygen created during polymeric network substitution, as discussed in [5,8].

3.4.2. Quantitative results

Following qualitative determination of the phases present in the fly ash, each phase was statistically defined, and a quantitative assessment was made to determine the relative proportions of each phase. First, using the supervised clustering analysis function of MultiSpec, user-defined training fields were specified for each phase. That is, for each phase qualitatively determined present, an example image area was selected which was representative of that phase. Following such definition of all phases, segmentation statistics were computed which delineated the statistical boundaries between phases.

The statistical boundary rules were then applied to the entire image, and each pixel was assigned to a phase based on those rules. A group of neighboring pixels was defined to form a "cluster", or fly ash particle, if the minimum cluster size was 3 pixels^2. Once 98% of the pixels had been assigned a phase and cluster, the image analysis was considered complete, a cluster map was generated showing the location of each cluster in the image, and a report was generated listing the relative proportion of each phase. The statistical probability of accurate classification was also computed for each phase. The cluster map is shown in Fig. 7.

Four samples were prepared and analyzed as described above. Multiple samples were analyzed to assess the level of precision to which each of the phase fractions could be measured. Each sample was taken from the same batch of fly ash, and was prepared independently of the others to account for error introduced through variability in sample preparation. The relative proportions of each of the phases for each of

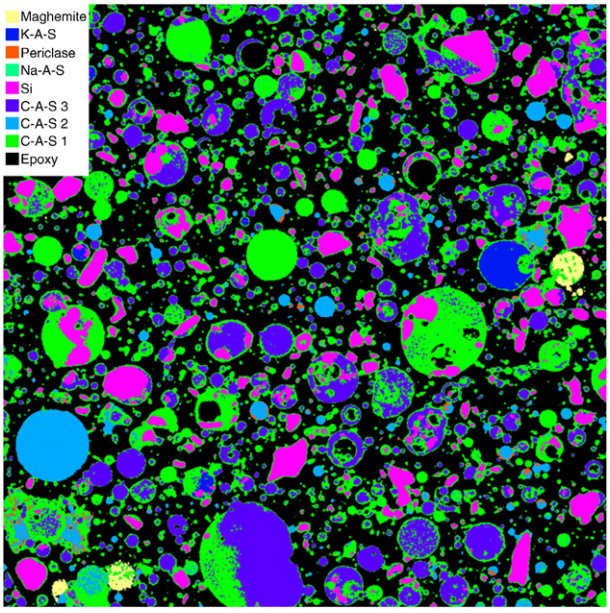

Fig. 7. Cluster map showing phase distinction in a Class F fly ash based upon multispectral analysis. Field width = 2050 μm.

the four samples are reported in Table 5, along with the range, mean value, and standard deviation for each phase. The area-fraction data determined through multispectral image analysis have been processed to yield proportions by mass for consistency with the XRD data.

After the relative proportions of each phase were determined, the composition of each of the phases was investigated. An image set was acquired and processed in the manner described above; however neither the field of view of the EDS nor the scan conditions were changed during image processing. Once a cluster map was generated showing the locations of the phases, the EDS was configured to collect an elemental spectrum of five points belonging to each phase, for a total of 40 individual spot analyses. The spot spectra were collected for 1 min each at an X-ray intensity of approximately 10,000 counts/s. The EDS system was calibrated with NIST reference standards K411 and K412 prior to the analysis. The results of the elemental analysis of each phase are presented in Table 6. The phase fractions may not total 100% due to traces of impurities present in the sample. The elemental analyses of quartz (SiO_2), maghemite (Fe_2O_3) and periclase (MgO) show the presence of elements other than the principal constituents of these phases. This is likely caused by substrate interference, as these crystalline phases are relatively small in size and are mixed within or deposited on the surface of the principal amorphous phases.

As previously stated, the inclusion of some crystalline phases in the MSIA allows comparison between the XRD and MSIA analyses. The bulk amorphous and crystalline fractions determined by each method may be compared, along with the individual crystalline phase fractions. Comparisons are made based upon the mean results of 5 replicate samples analyzed by XRD and single-fields of 4 replicate samples analyzed by MSIA. The bulk material comparison is shown in Table 6. It should be noted that the amorphous fraction as determined by MSIA may include microcrystalline mullite. However, this cannot be confirmed and the mullite fraction as determined by XRD was not subtracted from the bulk amorphous fraction or added to the bulk crystalline fraction as determined by MSIA to preserve the independence of the analytical methods. A comparison of the individual crystalline phase fractions as determined by the two analytical methods is shown in Table 7. The results obtained from each method are similar.

3.5. Discussion

The crystalline phases of the subject fly ash have been characterized by quantitative X-ray diffraction and the amorphous phases have been characterized by electron microscopy/energy dispersive spectroscopy coupled with multispectral image analysis. Qualitative crystalline phase analysis was perhaps the most objective analysis conducted, while quantitative analysis of crystalline phases and qualitative and quantitative analysis of amorphous phases proved subject to procedural details and analytical assumptions. Peculiarities and challenges of each method are discussed next, and a comparison of the two analytical methods is presented. The composition of the amorphous phases is also discussed.

Table 5
Relative proportions of crystalline and amorphous phases present in a Class F fly ash as determined by MSIA.

Phase	Relative amounts in samples (%)				Mean	Std. dev.
	1	2	3	4		
Quartz	17.4	17.9	17.5	18.0	17.7	0.3
Maghemite	2.4	3.2	2.8	2.6	2.8	0.4
Periclase	1.0	0.6	0.8	0.8	0.8	0.2
C-A-S 1	46.7	47.6	46.6	46.9	46.9	0.5
C-A-S 2	2.8	5.0	3.6	4.5	4.0	1.0
C-A-S 3	28.7	22.9	27.0	25.4	26.0	2.5
K-A-S	0.9	2.7	1.5	1.6	1.7	0.8
N-A-S	0.2	0.2	0.2	0.2	0.2	0.0

Table 6
Comparison of bulk phase composition between XRD and MSIA methods shows consistent estimates.[a]

Bulk phase	Phase amount (%), (std. dev.)	
	XRD	MSIA
Amorphous	77.3 (0.5)	78.8 (0.3)
Crystalline	22.7 (0.4)	21.6 (0.3)

[a] Based on 5 samples by XRD and 4 samples by MSIA.

Qualitative crystalline phase analysis was straightforward, as well-documented methods for crystalline phase identification and analysis were adapted and applied to fly ash. However, rigorous quantitative analysis of crystalline phases faced some obstacles. The largely amorphous composition of fly ash necessitated lengthy scan times to collect enough diffracted X-rays to sufficiently resolve representative peaks of minor phases. Even after unusually lengthy scans, peaks for mullite, maghemite, and periclase were poorly resolved. In the case of mullite, this may have been caused by poor ordering ("crystallinity") of the material. Mullite forms in fly ash by crystallization of molten aluminosilicate upon cooling in the flue gas stream. If the melt cools slowly enough to allow crystallization but too rapidly for the atoms to relax into their optimum crystalline configuration, a poorly-ordered, or poorly-crystalline structure will result. The diffraction process would thus be hindered, and diffraction peaks would be broader. In the cases of periclase and maghemite, low proportions relative to the bulk and overlap of peaks made precise intensity measurements difficult.

Both qualitative and quantitative analyses of the amorphous phases in the fly ash required some subjectivity and creativity. A sufficient sampling method had to be developed such that the phase proportions determined were representative of the bulk ash. This was accomplished by acquiring and analyzing EDS element maps of sizes ranging from 256 pixel^2 to 1024 pixel^2. Multiple image sets at each size were collected, each of a different field of view of the sample. Upon analysis, it was found that only as the image size approached 768 pixel^2 were the statistics similar from one image set to another. Conservatively, 1024 pixel^2 images were collected for this research. Analysis of four 1024 pixel^2 image sets shows very good agreement, and thus, one 1024 pixel^2 image was considered sufficient for amorphous phase investigation through multispectral image analysis for each specimen examined. Additionally, averaging multiple fields did not appear to yield substantial improvement in the results; therefore, a single field was deemed appropriate for sampling.

As expected, some of the crystalline phases were resolved through the multispectral image analysis and thus were included in the phase statistics. The detection of these phases proved useful in evaluating the accuracy of the analysis method, as the phase fractions determined through multispectral image analysis could be compared to those determined through Rietveld quantitative X-ray diffraction. Furthermore, the crystalline phase proportions could easily be excluded from the multispectral imaging results through renormalization. Crystalline maghemite and periclase were detected by SEM/EDS and well defined through the MSIA procedure; however, mullite was not.

Finally, the distinction between the individual amorphous phases should be discussed. As shown in Table 8, the alkali-modified glasses

Table 7
Comparison of individual crystalline phase composition between XRD and MSIA methods.[a]

Phase	Phase amount (%), (std. dev.)	
	XRD	MSIA
Quartz	16.4 (0.4)	17.7 (0.3)
Maghemite	2.1 (0.1)	2.8 (0.4)
Periclase	0.4 (0.0)	0.8 (0.2)

[a] Based on 5 samples by XRD and 4 samples by MSIA.

Table 8
Elemental analysis of phases in a Class F fly ash determined through semi-quantitative EDS, expressed as oxides.

Phase	Element	Oxide in sample (%)					Mean	Std. dev.
		1	2	3	4	5		
Quartz	SiO_2	99.3	95.3	98.0	99.3	95.2	98.0	2.1
	Al_2O_3	0.7	4.7	2.0	0.7	4.9	2.0	2.1
Maghemite	Fe_2O_3	93.1	92.9	93.0	93.1	92.6	92.9	0.2
	SiO_2	3.8	4.0	4.2	3.6	4.6	4.0	0.4
	Al_2O_3	2.4	2.1	2.4	2.4	1.9	2.2	0.2
	CaO	0.7	1.1	0.5	0.9	0.9	0.8	0.2
Periclase	MgO	87.9	88.2	88.2	94.4	86.6	89.1	3.0
	CaO	10.6	10.2	10.2	5.0	9.2	9.0	2.3
	Al_2O_3	1.4	0.9	0.9	0.6	3.1	1.4	1.0
	SiO_2	0.1	0.6	0.6	0.1	0.7	0.4	0.3
C-A-S 1	CaO	38.5	54.2	50.4	45.7	48.2	47.4	5.9
	Al_2O_3	37.8	31.3	33.7	41.8	31.8	35.3	4.4
	SiO_2	23.7	14.5	15.9	12.6	20.0	17.3	4.5
C-A-S 2	CaO	87.0	76.3	72.8	85.6	84.2	81.2	6.3
	Al_2O_3	8.5	17.2	16.6	9.8	8.0	12.0	4.5
	SiO_2	4.5	6.4	10.4	4.6	7.8	6.7	2.5
C-A-S 3	CaO	14.6	14.4	14.5	17.8	14.4	15.1	1.5
	Al_2O_3	68.4	67.2	64.7	63.7	69.9	66.8	2.6
	SiO_2	17.0	18.4	20.8	18.5	15.7	18.1	1.9
K-A-S	K_2O	68.3	72.9	75.9	77.2	73.7	73.6	3.4
	Al_2O_3	23.8	18.5	15.1	15.0	14.4	17.4	3.9
	SO_3	7.4	8.3	8.8	7.8	11.5	8.8	1.6
N-A-S	Na_2O	92.4	94.8	95.2	91.9	90.3	92.9	2.1
	Al_2O_3	5.2	3.6	3.9	5.2	7.4	5.1	1.5
	SiO_2	2.3	1.7	0.8	2.9	2.3	2.0	0.8

are largely composed of the alkali modifier, and thus may exhibit greater polymeric disorder than lesser-modified glasses. The calcium-modified glasses each exhibit vastly different CaO/SiO_2 and CaO/Al_2O_3 ratios, as shown in Table 9. For the purposes of this research, C-A-S 1 has been classified as an intermediate-calcium glass, C-A-S 2 has been classified as a high-calcium glass, and C-A-S 3 has been classified as a low-calcium glass.

The current research has led to development of new synergistic methods to characterize a Class F fly ash. During the course of the research, questions arose as to the applicability of these methods to other micro-scale civil engineering materials. Two materials, both commonly used in the production of concrete, were chosen on which to test these methods. Class C fly ash was selected for study, as it exhibits similar morphology to a Class F fly ash, but possesses more complex compositional characteristics. Furthermore, the proper characterization of Class C fly ash has wide implications on its use for mitigation of deleterious sulfate attack on concrete. Microfine aggregates were also selected for study. Their shape and chemical composition differ greatly from that of fly ash, but many possess more straightforward mineralogical characteristics. Microfine aggregates may significantly influence properties of both plastic and hardened concrete, including workability, strength, and durability. Preliminary case studies conducted to evaluate the applicability of the methods presented herein to the aforementioned materials yielded promising results. Details of the case studies are presented by Chancey [8].

Table 9
CaO/Al_2O_3 and CaO/SiO_2 ratios of the calcium-modified aluminosilicate glasses.

Glass	Ratio	Ratio in sample					Mean	Std. dev.	Classification
		1	2	3	4	5			
C-A-S 1	C/A	1.0	1.7	1.5	1.1	1.5	1.3	0.3	Intermediate-calcium
	C/S	1.6	3.8	3.2	3.6	2.4	2.7	0.8	
C-A-S 2	C/A	10.3	4.4	4.4	8.7	10.5	6.8	3.1	High-calcium
	C/S	19.3	11.9	7.0	18.8	10.8	12.0	5.3	
C-A-S 3	C/A	0.2	0.2	0.2	0.3	0.2	0.2	0.04	Low-calcium
	C/S	0.9	0.8	0.7	1.0	0.9	0.8	0.1	

4. Summary

Fly ash is an inherently heterogeneous coal-combustion by-product commonly used as a replacement of portland cement in concrete. Fly ash is a complex material, consisting of both crystalline and amorphous phases, each with unique reactivity in the concrete environment. A method of identifying and characterizing the discrete phases in this highly-variable, and often quite complex, material could lead to a better understanding of the influences of fly ash on concrete properties and thus result in a better quality end product.

Qualitative and quantitative methods were developed and refined to characterize the crystalline phases of a Class F fly ash. The relative proportions of the crystalline phases present in a Class F fly ash were determined through RQXRD. Accurate qualitative phase identification was necessary before quantification was possible, and detailed information regarding the crystalline structure of each phase was required for Rietveld analysis. The accuracy of results obtained through this method is subject to proper qualitative phase identification and proper refinement technique as described herein. Sample preparation for crystalline phase analysis is straightforward and relatively simple, facilitating the collection of large amounts of data. Qualitative analysis is quite time consuming for a given fly ash, as is preliminary Rietveld pattern refinement. However, once qualitative analysis and preliminary refinement are complete, the analytical process is straightforward and efficient.

The amorphous phases of a Class F fly ash were identified through MSIA of high-resolution element maps collected through SEM/EDS. Qualitative and semi-quantitative analyses of overlays of multiple element maps resulted in the determination of the number of mutually exclusive amorphous phases present in the fly ash, and identification of the location(s) of each of the phases. Elemental analysis of each phase yielded rough chemical compositions of each phase to confirm its exclusivity from the others. Results obtained through the use of this method are quite subjective because they depend on user-defined constraints on the statistical image analysis. Statistical parameters may be defined such that an almost infinite number of phases may be identified based upon infinitesimal differences in elemental composition. Parameters must be selected and subsequent analyses tested such that phase delineations appear reasonable and yield results of appropriate complexity for the research at hand.

Sample preparation for amorphous phase analysis is more complex and far more time consuming than that for crystalline phase analysis. Polished section preparation and SEM/EDS analysis is a multi-step process completed over a period of days. A suitable SEM/EDS system should be carefully selected, and a subset of samples should be chosen to minimize costly equipment usage.

Acknowledgements

Funding for this research was provided through a National Science Foundation Graduate Research Fellowship to one of the authors (RTC) and a grant from the International Center for Aggregates Research (ICAR). The authors would like to thank Dr. Edward Garboczi, Dr. Kevin Folliard, and Dr. Yangming Sun for fruitful conversations and guidance through the research process. Thanks are also due to Mr. Chance Kutac and Ms. Julia Rager, both undergraduate research assistants at the University of Texas at Austin, for endless hours preparing samples for microanalysis.

References

[1] American Coal Ash Association, Fly Ash Facts for Highway Engineers, Fourth EditionFederal Highway Administration, Washington, DC, 2003.
[2] ASTM Standard C 618, Standard Specification for Coal Fly Ash and Raw or Calcined Natural Pozzolan for Use as a Mineral Admixture in Concrete, Annual Book of ASTM Standards, ASTM International, West Conshohocken, PA, 2005.
[3] W.C. McKerall, W.B. Ledbetter, D.J. Teague, Analysis of Fly Ashes Produced in Texas. 1982, Texas Transportation Institute, Texas A&M University: College Station, TX.

[4] R.T. Hemmings, E.E. Berry, On the Glass in Coal Fly Ashes: Recent Advances, Materials Research Society Symposium Proceedings, vol. 113, Materials Research Society, Pittsburgh, 1988.
[5] H.S. Pietersen, Reactivity of Fly Ash and Slag in Cement. Ph.D. Dissertation, Delft University of Technology, Delft, The Netherlands. 1993.
[6] S. Mindess, J.F. Young, D. Darwin, Concrete, 2nd edPrentice Hall, Upper Saddle River, NJ, 2003.
[7] S. Schlorholtz, K. Bergeson, T. Demirel, Monitoring Fluctuations in the Physical and Chemical Properties of a High-Calcium Fly Ash, Materials Research Society Symposium Proceedings, vol. 113, Materials Research Society, Boston, 1987.
[8] R. Chancey, Characterization of Crystalline and Amorphous Phases and Respective Reactivities in a Class F Fly Ash. Ph.D. Dissertation, The University of Texas at Austin, Austin, TX. 2008.
[9] G.J. McCarthy, J.K. Solem, O.E. Manz, D.J. Hassett, Use of a Database of Chemical, Mineralogical, and Physical Properties of North American Fly Ash to Study the Nature of Fly Ash and its Utilization as a Mineral Admixture in Concrete, Materials Research Society Symposium Proceedings, vol. 178, Materials Research Society, Boston, 1989.
[10] G.J. McCarthy, X-ray Powder Diffraction for Studying the Mineralogy of Fly Ash, Materials Research Society Symposium Proceedings, vol. 113, Materials Research Society, Pittsburgh, 1988.
[11] G.J. McCarthy, K.D. Swanson, L.P. Keller, W.C. Blatter, Mineralogy of western fly ash, Cement and Concrete Research 14 (4) (1984) 471–478.
[12] B.E. Scheetz, W.B. White, Characterization of Crystalline Phases in Fly Ash by Microfocus Raman Spectroscopy, Materials Research Society Symposium Proceedings, vol. 43, Materials Research Society, Boston, 1985.
[13] C.R. Ward, D. French, Determination of glass content and estimation of glass composition in fly ash using quantitative X-ray diffractometry, Fuel 85 (16 SPEC ISS) (2006) 2268–2277.
[14] C.R. Ward, D. French, Relation Between Coal and Fly Ash Mineralogy Based on Quantitative X-ray Diffraction Methods, World of Coal Ash Conference, World of Coal Ash, Lexington, KY, 2005 Accessed Online: http://www.flyash.info/2005/209war.pdf.
[15] R.S. Winburn, Development of the Rietveld Method for Quantitative X-ray Diffraction Analysis of Complex Mixtures Including Coal Combustion By-Products. Ph.D. Dissertation, North Dakota State University, Fargo. 1999.
[16] R.S. Winburn, D.G. Grier, G.J. McCarthy, R.B. Peterson, Rietveld quantitative X-ray diffraction analysis of NIST fly ash standard reference materials, Powder Diffraction 15 (3) (2000) 163–172.
[17] R.S. Winburn, D.G. Grier, B.R. Jarabek, G.J. McCarthy, Quantitative XRD Analysis of Coal Combustion By-Products by the Rietveld Method I. Database, 46th Denver X-ray Conference, Denver, 1997.
[18] R.S. Winburn, S.L. Lerach, G.G. McCarthy, D.G. Grier, J.D. Cathcart, Quantification of ferrite spinel and hematite in fly ash magnetically enriched fractions, Advances in X-ray Analysis 43 (2000) 350–355.
[19] B. Mather, The glass in low-calcium fly ash, Cement and Concrete Research 14 (1984) 887–890.
[20] P.J. Williams, J.J. Biernacki, C.L. Rawn, L. Walker, J. Bai, Microanalytical and computational analysis of class f fly ash, ACI Materials Journal 102 (5) (2005) 330–337.
[21] H.M. Rietveld, A profile refinement method for nuclear and magnetic structures, Journal of Applied Crystallography 2 (1969) 65–71.
[22] Q.I. Roode-Gutzmer, Y. Ballim, Phase Composition and Quantitative X-ray Powder Diffraction Analysis of Portland Cement and Clinker, American Ceramic Society, Westerville, OH, 2001.
[23] R.A. Young, The Rietveld Method, International Union of Crystallography monographs on crystallography, Oxford University Press, Oxford, 1993.
[24] D.M. Kerrick, The role of carbon film thickness in electron microprobe analysis, American Mineralogist 58 (1973) 920–925.
[25] J. Goldstein, Scanning Electron Microscopy and X-ray Microanalysis, 3rd ed.Kluwer Academic/Plenum Publishers, New York, 2003.
[26] J.W. Lydon, The Measurement of the Modal Mineralogy of Rocks From SEM Imagery: The Use of MultiSpec and ImageJ Freeware, Geological Survey of Canada, 2005 Open File 4941. p. 37p.
[27] W. Rasband. ImageJ: Image Processing and Analysis in Java. [Technical Documentation] 2004 October 31, 2007 [cited; Available from: http://rsb.info.nih.gov/ij/index.html.
[28] D.P. Bentz, S. Rémond, Incorporation of Fly Ash into a 3-D Cement Hydration Microstructure Model, National Institute of Standards and Technology, Gaithersburg, MD, 1997.
[29] J.E. Shelby, Introduction to Glass Science and Technology, 2nd ed.Royal Society of Chemistry, Cambridge, 2005.
[30] R.T. Hemmings, E.E. Berry, Speciation in Size and Density Fractionated Fly Ash, Materials Research Society Symposium Proceedings, vol. 65, Materials Research Society, Pittsburgh, 1986.
[31] J.C. Qian, F.P. Glasser, Bulk Composition of the Glassy Phase in Some Commercial PFA's, Materials Research Society Symposium Proceedings, vol. 113, Materials Research Society, Boston, 1987.
[32] Headwaters Resources, Report of Fly Ash Limestone Plant, Jewett, Texas Unit #1,2. 2005: Jewett, TX.
[33] International Center for Diffraction Data, Powder Diffraction File: Inorganic Phases, Data Book, Newtown Square, ICDD, PA, 1996.